Predictability of summer northwest Pacific climate in 11 coupled model hindcasts: Local and remote forcing

J. S. Chowdary,[1] Shang-Ping Xie,[1] June-Yi Lee,[1] Yu Kosaka,[1] and Bin Wang[1]

Received 8 June 2010; revised 20 August 2010; accepted 8 September 2010; published 30 November 2010.

[1] The skills of 11 coupled ocean-atmosphere general circulation models (CGCMs) are investigated in the prediction of seasonal rainfall and circulation anomalies over the northwest (NW) Pacific for the period 1980–2001, with a focus on the summer following the mature phase of El Niño (hereafter JJA(1)). It is shown that the first empirical orthogonal function (EOF) mode of sea level pressure is closely tied to the second EOF mode of rainfall variability over the NW Pacific during JJA(1), indicative of strong feedback between circulation and convection. Most coupled models and the associated multimodel ensemble well predict these EOF modes and their relationship with high fidelity. Coupled models are capable of predicting suppressed rainfall over the NW Pacific in JJA(1). A few models fail to predict the concurrent weak negative sea surface temperature (SST) anomalies on the southeastern flank of the anomalous anticyclone. This suggests that remote forcing via teleconnections is important for NW Pacific rainfall prediction in those models. In some models, local air-sea interactions seem also to play a role. Specifically, remote forcing by tropical Indian Ocean (TIO) SST variability is identified as influential on NW Pacific climate during JJA(1). TIO SST affects the atmosphere over the NW Pacific by two mechanisms, via the equatorial Kelvin wave and the intensification of the subtropical westerly jet. Overall, models are successful in predicting the antisymmetric patterns of precipitation and winds over TIO during spring, which are critical in sustaining the TIO warming through the subsequent summer.

Citation: Chowdary, J. S., S.-P. Xie, J.-Y. Lee, Y. Kosaka, and B. Wang (2010), Predictability of summer northwest Pacific climate in 11 coupled model hindcasts: Local and remote forcing, *J. Geophys. Res.*, *115*, D22121, doi:10.1029/2010JD014595.

1. Introduction

[2] Over much of East Asia summer (June–July–August, JJA) is the principal rainy season. Interannual variability of East Asia summer rainfall is strongly linked with that of subtropical high pressure in the northwest (NW) Pacific [e.g., *Chang et al.*, 2000; *Wang et al.*, 2003; *Huang et al.*, 2004]. The delayed impact of El Niño-Southern Oscillation (ENSO) on East Asia/NW Pacific summer climate is complex. Typically, El Niño develops during boreal summer, peaks during early winter, and decays in the following spring. The sea surface temperature (SST) anomalies of El Niño do not persist to the following summer in the east/central Pacific and therefore, have little direct effect on the NW Pacific atmosphere. Persistent atmospheric anticyclone anomalies from El Niño winter to summer over the NW Pacific involve interactions with negative SST anomalies to the southeast, especially during winter [*Wang et al.*, 2000]. Several studies demonstrate that local SST anomalies are not the sole forcing for convection during summer in the NW Pacific [*Lu*, 2001; *Lee et al.*, 2008; *Li et al.*, 2008; *Xie et al.*, 2009; *Wu et al.*, 2010]. Furthermore, *Xie et al.* [2009] suggest that the remote forcing from the tropical Indian Ocean (TIO) is important for rainfall variability over the NW Pacific during summer following El Niño. Hereafter, we denote summers during the developing and decay years of El Niño as JJA(0) and JJA(1), respectively. In the recent decades after the late 1970s, the ENSO teleconnection at its decay phase strengthens over the Indo-western Pacific [*Wang et al.*, 2008], for which the enhanced TIO warming again holds the key [*Xie et al.*, 2010].

[3] The winter El Niño causes the TIO to warm [*Klein et al.*, 1999]. This TIO warming persists into the summer monsoon season [*Yang et al.*, 2007; *Du et al.*, 2009; *Park et al.*, 2010]. Over the NW Pacific, the anticyclonic anomalies in the lower troposphere originate during the fall of the El Niño development [*Wang and Zhang*, 2002; *Lau and Nath*, 2003], intensify during the mature El Niño phase and the ensuing spring, and persist and slowly decay through the following summer [*Wang et al.*, 2003]. This anomalous summer anticyclone is important for rainfall variability over East Asia/NW Pacific [*Shen et al.*, 2001; *Huang et al.*, 2004; *Li et al.*, 2008; *Kripalani et al.*, 2010; *Xie et al.*, 2009; *Chowdary et al.*, 2010]. An interaction between the persistent TIO SST warming and summer NW Pacific anticyclone is

[1]International Pacific Research Center, University of Hawaii at Manoa, Honolulu, Hawaii, USA.

0148-0227/10/2010JD014595

Table 1. Description of the Models Used in the Study

Abbreviation	Institute	AGCM	OGCM	Ensemble Number; Period	Reference
BMRC	BMRC-POAMA1.5	BAM 3.0d T47 L17	ACOM2 0.5–1.5°lat 2°lon L31	10; 1980–2002	*Hudson et al.* [2010]
CERF	CERFACS	ARPEGE T63L31	OPA 8.2 2° lat 2°lon L31	9; 1980–2001	*Palmer et al.* [2004]
ECMW	ECMWF	IFS T95L40	HOPE-E 0.3–1.4° lat 1.4°lon L29	9; 1980–2001	*Palmer et al.* [2004]
GFT1	GFDL	AM2.1 2°lat 2.5°lon L24	OM3.1 (MOM4) 1/3°lat 1°lon L50	10; 1979–2005	*Delworth et al.* [2006]
INGV	INGV	ECHAM4 T42L19	OPA8.1 0.5–1.5°lat 2°lon L31	9; 1980–2001	*Palmer et al.* [2004]
LODY	LODYC	IFS T95L40	OPA8.2 2° lat 2°lon L31	9; 1980–2001	*Palmer et al.* [2004]
METF	Météo-France	ARPEGE T63L31	OPA 8.0 182 GP × 152 GP L31	9; 1980–2001	*Palmer et al.* [2004]
MAXP	MPI	ECHAM-5 T42L19	MPI-OM1 0.5–2.5°lat 2.5°lon L23	9; 1980–2001	*Palmer et al.* [2004]
NCEP	NCEP	CFS T62 L64	MOM3 1/3°lat 1°lon L40	15; 1981–2004	*Saha et al.* [2006]
SINT	FRCGC-SINTEX-F	ECHAM4 T106 L19	OPA 8.2 2°cos(lat) 2°lon L31	9; 1982–2004	*Luo et al.* [2005]
UKMO	Met Office	HadAM3 2°lat 3.75°lon L19	GloSeaOGCM 0.3–1.25°lat 1.25°lon L40	9; 1980–2001	*Palmer et al.* [2004]

proposed by *Xie et al.* [2009] through an atmospheric Kelvin wave-induced Ekman divergence (WIED) mechanism. The TIO surface warming causes tropospheric temperature to increase via deep convection, emanating a baroclinic Kelvin wave into the equatorial Pacific. The warm Kelvin wave wedge lowers the sea level pressure (SLP) in the equatorial western Pacific, inducing northeasterly surface wind anomalies over the subtropical NW Pacific. The resultant divergence in the subtropics suppresses convection and the convective and circulation anomalies amplify via their interaction. Thus, a strong TIO response translates into a pronounced development of atmospheric anomalies over the NW Pacific and East Asia during JJA(1) as the direct influence of ENSO fades away.

[4] The above mechanism is supported by coupled ocean-atmosphere forecast model experiments [*Chowdary et al.*, 2010]. By replacing TIO SST with climatology, atmospheric anomalies such as the anticyclonic circulation over the NW Pacific weaken by 50% during JJA(1). Thus, additional predictability can be obtained by considering the TIO SST variability into account. The present study tests the Kelvin WIED mechanism for the TIO influence on the NW Pacific in a suite of coupled model retrospective forecasts and the associated multi model ensemble (MME). It is worth noting that treating summer monsoon as a passive response to the underlying SST forcing and the use of atmospheric general circulation models to examine the response may be inadequate because the SST anomalies over the monsoon region often lags precipitation anomalies, suggesting that the former are the result of the latter [*Wang et al.*, 2004, 2005]. This study uses coupled climate models to represent atmosphere-ocean interactions in interannual variations. Specifically, we examine forecasts from 11 coupled models for 1980–2001 and their skill in capturing NW Pacific atmospheric circulation anomalies and the relevant teleconnection patterns. Our goal is twofold: to assess the predictability of NW Pacific climate variability in summer following El Niño in the 11-model ensemble, and to investigate role of local and remote forcing in predicting NW Pacific atmospheric anomalies.

[5] Key to predicting NW Pacific atmospheric anomalies during JJA(1) are SST anomalies, both local and over the TIO. Two mechanisms are identified for TIO to affect NW Pacific rainfall variability during JJA(1) remotely. One is the Kelvin wave-induced Ekman divergence mechanism [*Xie et al.*, 2009] and the other is through the intensification of the subtropical westerly jet, both in response to the TIO warming. This study also shows that most models are successful in predicting the antisymmetric patterns of precipitation and winds over TIO during spring as they are essential to maintaining the TIO warming through the subsequent summer. The paper is organized as follows. Section 2 describes data and models used in the study. Section 3 presents a statistical evaluation of models in terms of capturing leading modes and teleconnection patterns. Section 4 discusses the impact of local and remote forcing on NW Pacific summer climate and the underlying physical mechanisms. Section 5 evaluates the prediction of the TIO spring asymmetric mode and early summer rainfall over the NW Pacific at long lead times. Section 6 provides a summary.

2. Data and Models Used

[6] The hindcast data set is derived from 11 global coupled ocean-atmospheric general circulation models (CGCMs) (see Table 1). They include seven coupled models from the European Center's Development of a European MultiModel Ensemble System for Seasonal to Inter-Annual Prediction (DEMETER) database [*Palmer et al.*, 2004] and four coupled models from the Asian-Pacific Economic Cooperation Climate Center (APCC)/Climate Prediction and its Application to Society (CliPAS) project [*Wang et al.*, 2009]. We use coupled model integrations initialized from 1 May and 1 February at 1 and 4 month lead time seasonal predictions for the common period of 1980–2001 for nine models. Note that the multi model ensemble in this study is based on the period of 1982–2001 as the SINTEX-F hindcast is available only for the shorter period. The NCEP-CFS hindcast is available from 1981. For detailed information of individual models, and their initial conditions, see *Wang et al.* [2009] and *Lee et al.* [2010]. For each model, ensemble-mean anomalies are calculated based on the monthly ensemble-mean climatology for each lead time.

[7] Model results are compared with the Hadley Centre sea ice and sea surface temperature (HadISST) data [*Rayner et al.*, 2003], the National Centers for Environmental Prediction (NCEP) reanalysis 2 [*Kanamitsu et al.*, 2002] SLP, geopotential height and wind data at the 850 and 200 hPa levels and the Center for Climate Prediction merged analysis for precipitation (CMAP) [*Xie and Arkin*, 1996] data. Tropospheric temperature is represented by the geopotential height difference between 200 and 850 hPa. Various statis-

Table 2. Lag Correlation Between First JJA SLP PC (EOF-1) and NDJ Niño 3.4 and Second JJA Rainfall PC (EOF-2) and NDJ Niño 3.4[a]

Observations and Models	Correlation Between JJA SLP PC-1 and NDJ Niño 3.4	Correlation Between JJA Rainfall PC-2 and NDJ Niño 3.4
Observed	0.52	0.64
CERF	0.69	0.66
ECMW	0.47	0.72
INGV	0.46	0.68
LODY	0.34	0.65
MAXP	0.41	0.25
METF	0.73	0.75
UKMO	0.32	0.35
BMRC	0.82	0.74
NCEP	0.80	0.83
GFT1	0.73	0.78
SINT	0.63	0.66
MME	0.71	0.75

[a]Model 1 month lead prediction is used. JJA, June–July–August; NDJ, November–December–January.

tical methods are used such as empirical orthogonal function (EOF), correlation, regression and composite analysis to evaluate model skill and to determine the physical mechanisms. Correlation coefficient r = 0.43 is significant at the 95% confident level for 22 years based on a two-tailed student's *t* test. Seasons are defined as those of the Northern Hemisphere.

3. Dominant Modes of East Asian-Northwest Pacific Climate and ENSO Teleconnection

3.1. Dominant Modes of SLP and Rainfall Over the East Asian/NW Pacific

[8] EOF analysis is used to identify the dominant modes of interannual SLP and precipitation variability over the NW Pacific during JJA. The first EOF (EOF-1) mode of JJA SLP and the second EOF (EOF-2) mode of JJA rainfall are associated with the summer following the mature phase of El Niño in both observations and 1 month lead predictions, as in work by *Xie et al.* [2009] and *Chowdary et al.* [2010]. Lag correlation between the first EOF (PC-1) of JJA SLP with NDJ Niño3.4 is 0.52 for observations and 0.71 for MME. In the case of the second EOF (PC-2) of JJA rainfall with NDJ Niño3.4, correlation is 0.64 for observations and 0.75 for MME. Table 2 provides lag correlations of individual modes for both SLP and rainfall PCs with NDJ Niño3.4. In most models the correlations are significant. Figures 1 and 2 show the spatial patterns of SLP EOF-1 and rainfall EOF-2 for observations, for individual coupled models, and for the MME at 1 month lead times. The regressed pattern of 850 hPa horizontal winds (vectors) against the first principal component (PC-1) of SLP is also displayed in Figure 1. There are similarities and differences in the NW Pacific SLP, low-level circulation and rainfall (Figures 1 and 2) among the models compared with observations. Most models (including MME) displayed an SLP spatial pattern similar to that of observations over the NW Pacific. The observed EOF-1 for SLP exhibits a NW Pacific high with an extension toward the East Asian landmass, with the largest loading around 20°N and 150°E. In some models (LODY, MAXP and SINT) the SLP mode has the maximum loading around 130°E and does not extend farther west. The pattern correlation of SLP EOF with observations is high, exceeding 0.6 in all models (the top of each panel of Figure 1). Even though the temporal correlation between the model PCs and the observed PC is slightly less than the pattern correlation, it stays above 0.43, exceeding the 95% confidence level (Figure 1n). The MME shows better skill in both pattern and temporal correlations than most of individual models.

[9] Many models are in qualitative agreement with observations in terms of strength and magnitude of the anticyclonic circulation over the NW Pacific. Unlike the tropical region, anomalous winds are weaker in the northern flank of the anticyclone in most models compared with observations. The anomalous anticyclone is consistent with the rainfall distribution and suggestive of a feedback between circulation and rainfall (Figures 1 and 2). In comparison with observations, there is a southward displacement of positive rainfall anomalies over the Japan in most models (Figure 2). Many models produce too much rain over the western equatorial Pacific while negative precipitation anomalies are underestimated over the South China Sea during JJA(1). The latter is the bias associated with the underestimation of the strength and westward extension of the anticyclone. Warm SST anomalies in the South China Sea appear to contribute to the rainfall bias [*Chowdary et al.*, 2010], as atmospheric feedback plays a major role in determining local SST over this region [*Wang et al.*, 2005].

[10] The pattern correlation for precipitation second EOF with observations stays above 0.44 in all models, except in MAXP over the NW Pacific (Figure 2). The temporal correlation between the model PCs and observed PC also exceeds 0.43 in most models, significant at the 95% confidence level. The MME shows superior skill in terms of the pattern correlation compared with individual models. Except MAXP, all models display reasonable skill in predicting the JJA(1) rainfall over the NW Pacific at a lead time of 1 month. Those models with weak SLP/wind response display poor precipitation prediction skill over the NW Pacific (Figures 1 and 2).

[11] The second mode for JJA rainfall is closely related with the first mode for JJA SLP. Figure 3 shows that the correlation coefficient between the SLP PC-1 (PC-2) and the rainfall PC-2 (PC-1) is 0.81 (0.53) for observations and 0.95 (0.84) for the MME prediction. This correlation measures the circulation-convection (CC) feedback in the NW Pacific, illustrating the importance of local feedback [*Xie et al.*, 2009] for the prediction of interannual variability in this region. Anomalies in Figures 1 and 2 are indicative of a consistent relationship between circulation and rainfall. Subtropical divergence suppresses convection, and suppressed convection intensifies the surface divergence. The ensuing feedback between convection and circulation amplifies anomalies of both fields, and gives rise to a strong anomalous anticyclone in the lower troposphere [*Xie et al.*, 2009]. Some models (LODC, and MAXP) far underestimate the relationship (Figure 3). These models tend to have low skill for the second rainfall PC (Figure 2n).

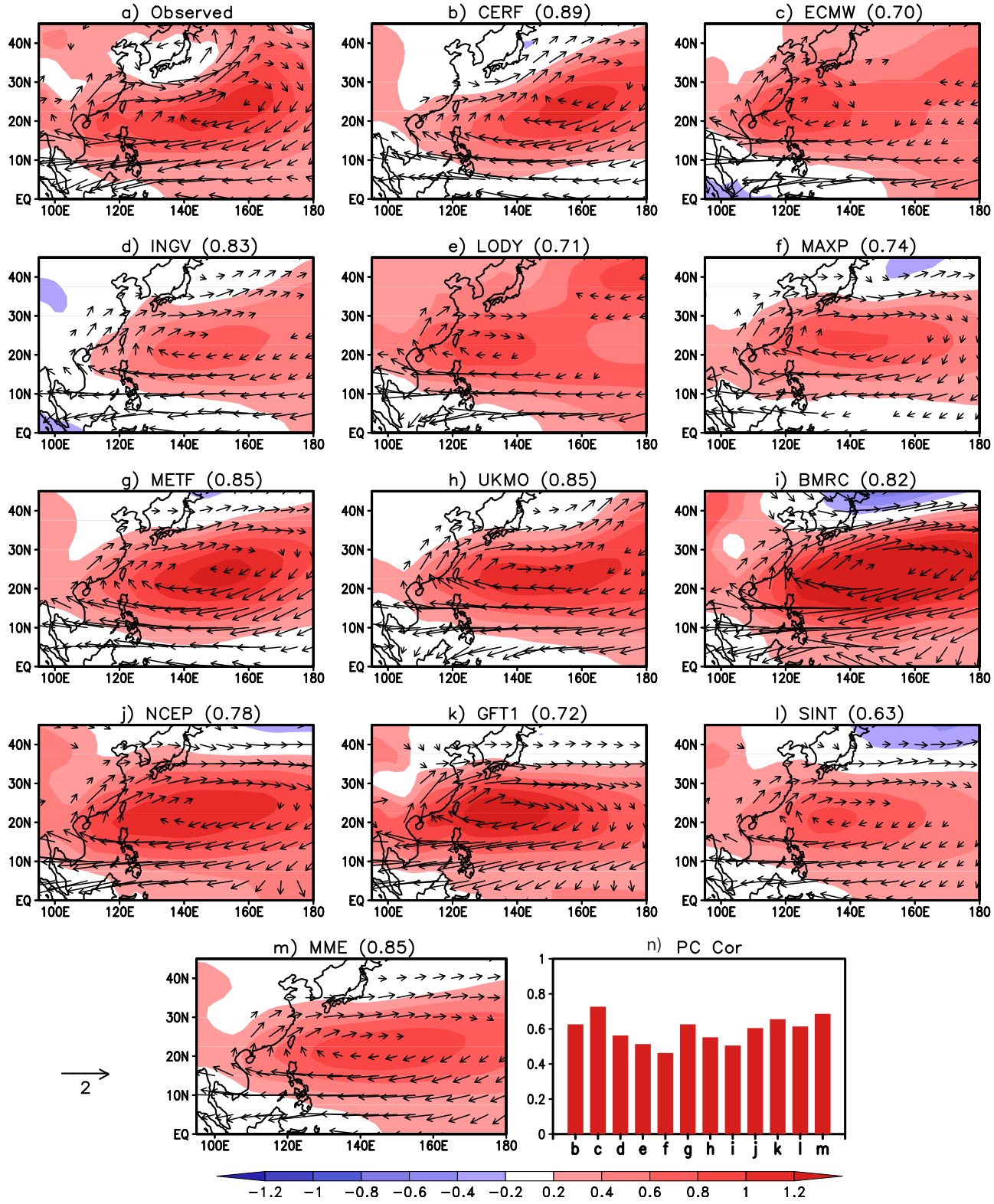

Figure 1. The first EOF of JJA SLP anomalies (hPa) obtained from (a) observations, (b–l) individual coupled models, and (m) MME (1 month lead prediction). (n) Temporal correlation in PC between observations and each model. In Figures 1a–1m, vectors represent the 850 hPa wind anomalies (m s^{-1}) regressed against the corresponding SLP PC. The pattern correlation between the observed and predicted EOFs is shown at the top of Figures 1b–1m.

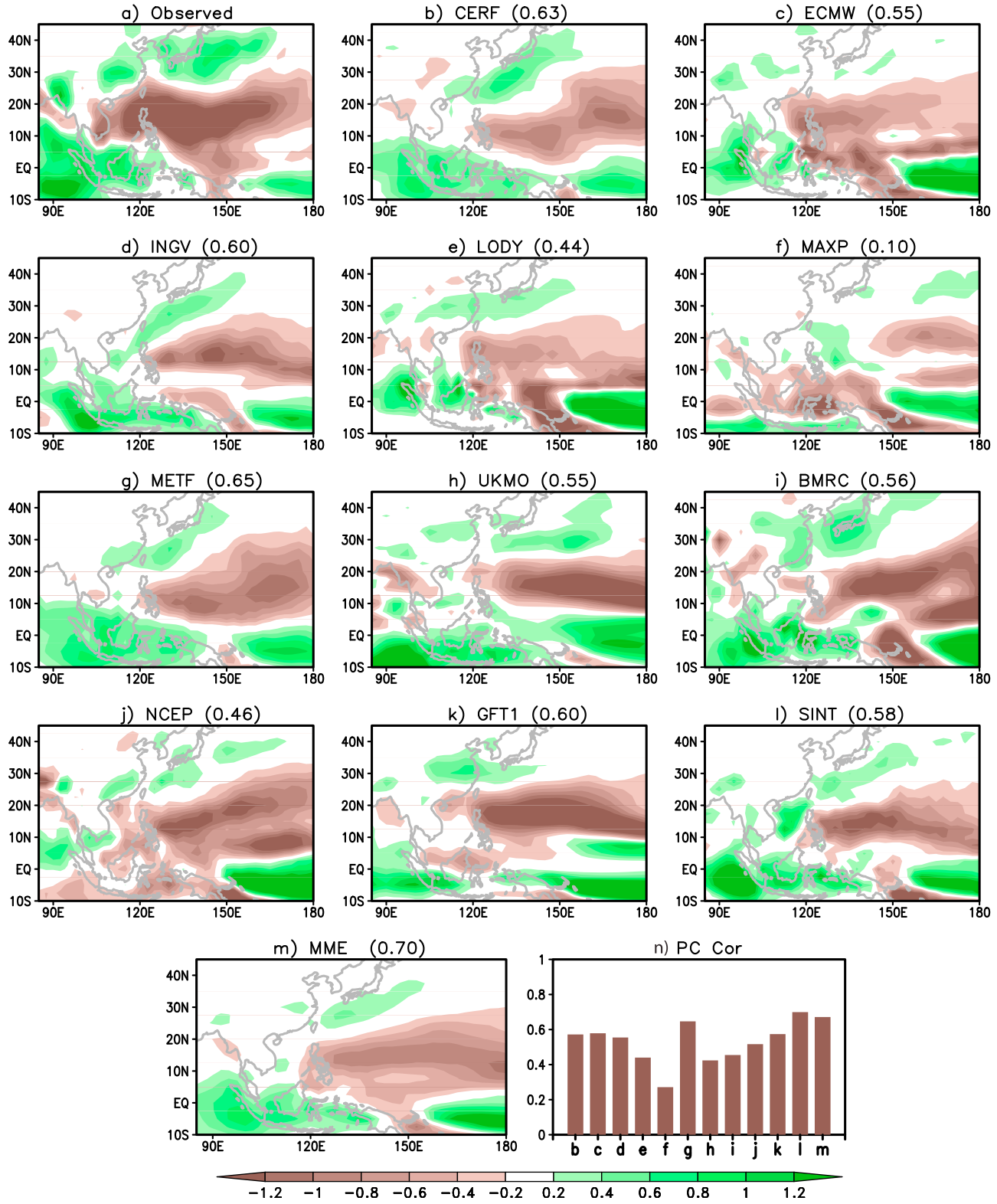

Figure 2. Same as Figure 1 but for the second EOF mode of JJA precipitation (mm/d) anomalies.

3.2. ENSO Teleconnection

[12] Here we examine the ENSO teleconnection to the Indo-western Pacific during summer. Figure 4 shows the correlation between JJA(1) Indo-western Pacific SST, SLP and 850hPa winds with the NDJ(0) (November(0)-December(0)-January(1)) Niño 3.4 index. Most models capture positive SST correlations over the western and northern Indian Ocean (NIO), consistent with observations. A few models show

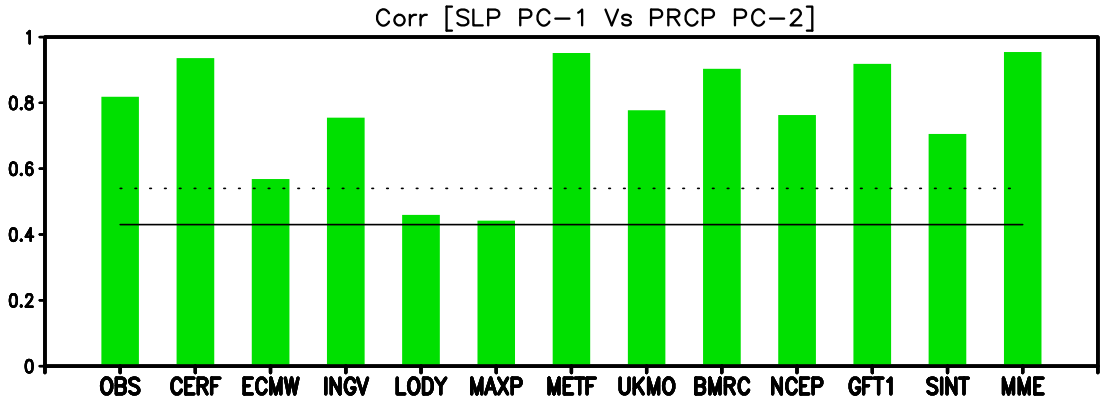

Figure 3. Correlation between the NW Pacific SLP PC-1 and precipitation PC-2 for observations, individual models, and MME based on 1 month lead prediction. Solid and dotted lines represent 95% and 99% confidence levels, respectively.

strong positive correlation over the east equatorial Indian Ocean and South China Sea (INGV, METF and BMRC). Many models reproduce the SLP correlation distribution over the NW Pacific for 1 month lead prediction. The NW Pacific 850hPa wind correlation closely resembles that of the regression against SLP PC-1, as both are characterized by anticyclonic circulation pattern. The comparison between models and observations reveals considerably better prediction of the basin-scale warming over the TIO than of rainfall (Figures 4 and 5). This highlights that the prediction of teleconnected precipitation is a very challenging problem with the current coupled models.

[13] All models show the negative correlation of precipitation on the southeast flank of the 850 hPa anticyclonic anomalies in the NW Pacific in JJA(1) when correlated with the NDJ(0) Niño-3.4 index (Figure 5). This supports the view that the suppressed convection to the southeast of the NW Pacific anticyclonic anomalies can reinforce the circulation [*Wang et al.*, 2000]. At the same time, there are positive rainfall correlations over the Indian Ocean, east China and Japan. Negative SST anomalies are very weak over the NW Pacific during JJA(1) as shown in observations (Figure 4a). One third of the models fail to predict the weak negative SST anomaly but are able to forecast the suppressed rainfall in the subtropical NW Pacific (e.g., NCEP and SINT). This suggests that the remote forcing via teleconnections is important for precipitation prediction in those models over the NW Pacific region. In a few models, the strong SST cooling on the southeastern flank of anomalous anticyclone is noticed (e.g., BMRC and GFT1), which is an important component for enhancing local air-sea interaction in JJA(1).

[14] As noted in previous studies [*Xie et al.*, 2009, 2010; *Chowdary et al.*, 2010], the tropospheric temperature (TT) response to the TIO warming (Figure 5) displays the *Matsuno* [1966]-*Gill* [1980] pattern, with a Rossby wave response over the TIO and an equatorial Kelvin wave response that penetrates into the west equatorial Pacific. The Kelvin wave response, in particular, is important in triggering surface divergence on the southwestern flank of the NW Pacific anticyclone [*Xie et al.*, 2009]. Upper-level (200 hPa) winds show significant variations over the Indo-western Pacific during JJA(1) when correlated with the NDJ(0) Niño-3.4 index (Figure 5), whose effects are discussed in section 4. In a few models, the teleconnection patterns are unrealistic, as represented by correlations with NDJ(0) Niño-3.4 SST. For example in MAXP rainfall anomalies are weak over the NW Pacific, and TT anomalies display too broad meridional structures in the Pacific.

4. Role of Local and Remote Forcing on NW Pacific Summer Rainfall

4.1. Effect of Local SST Cooling

[15] In observations (Figure 4a), the JJA(1) SST anomaly correlations with NDJ Nino3.4 are strong over the TIO but are of marginal significance over the NW Pacific. SST cooling on the southeastern flank of the anticyclone is weak in some models (INGY, MAXP, NCEP and SINT) and strong in some other models (CERF, METF, BMRC and GFT1). In the former models, the surface anticyclone develops in the absence of local SST cooling while in latter models, local air-sea interaction, with negative SST anomalies suppressing convection, is important during the summer following El Niño [*Wang et al.*, 2000]. We examine the relationship between NW Pacific summer circulation and local and TIO SST.

[16] Figure 6 shows correlation of SST and 850 hPa winds averaged over 5°N–20°N with the NW Pacific JJA SLP PC-1 for observations, individual models and the MME. Initialized from 1 May, a few models display a gradual decay of negative SST anomalies from May(1) to August(1) over the NW Pacific. Models like CERF, METF, BMRC and GFT1 display relatively strong cooling east of the anomalous anticyclone. The negative SST anomalies located on the southeastern flank of the anomalous anticyclone help to maintain the circulation anomalies by suppressing convection and exciting a descending atmospheric Rossby waves [*Wang et al.*, 2000, 2003]. This local ocean-atmospheric interaction may play an important role in the maintenance of the NW Pacific anticyclone during winter and spring. As the positive air-sea feedback over this region weakens from summer onward, the negative SST anomalies gradually decay and weaken the local forcing of convection anomalies as summer progresses

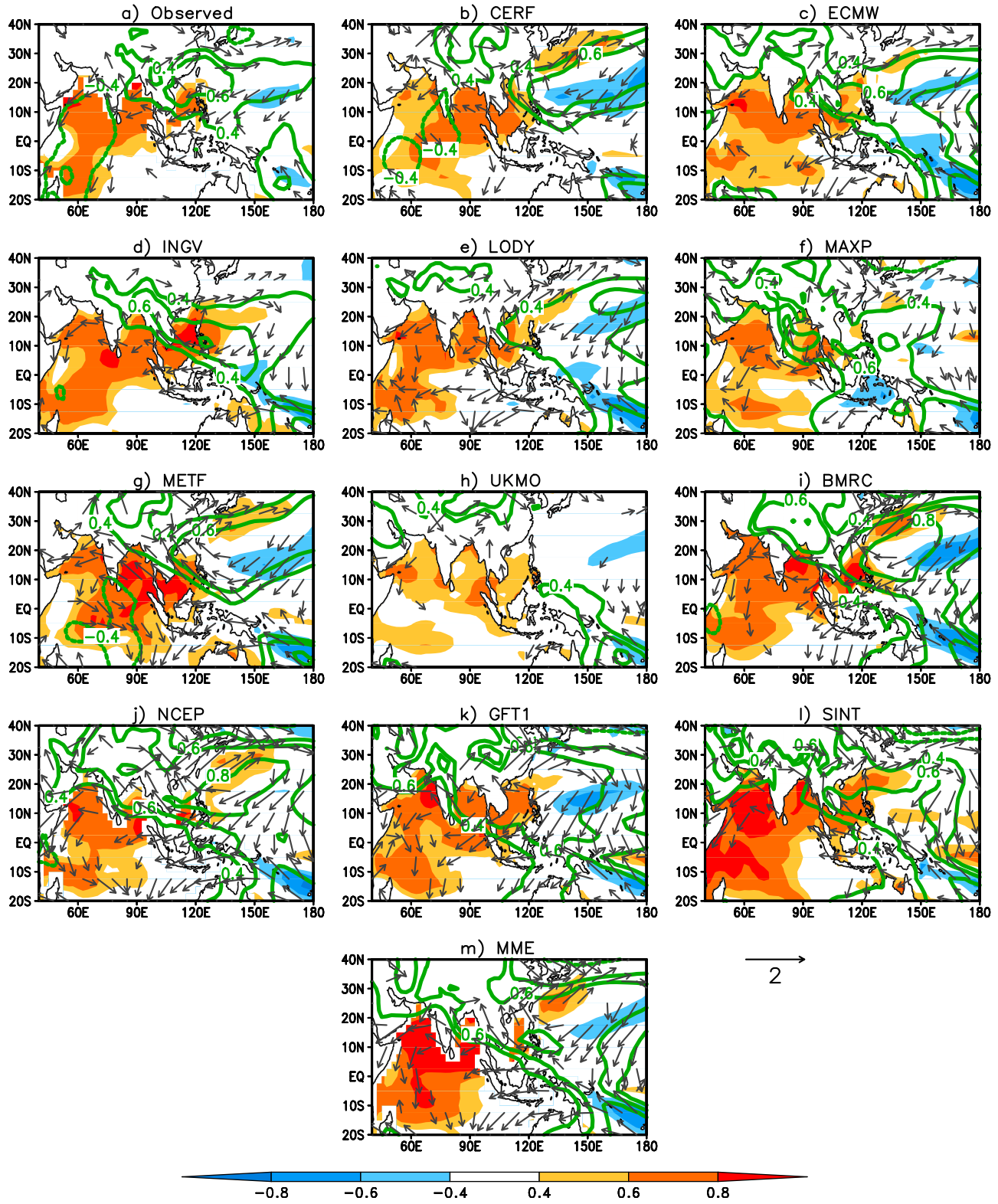

Figure 4. NDJ(0) Niño-3.4 SST index correlation with JJA(1) SST (shaded), SLP (contours), and 850 hPa wind velocity (vectors) for (a) observations, (b–l) individual models, and (m) MME at 1 month lead prediction.

[*Wu et al.*, 2010]. Some models (ECMW, LODY and UKMO) display a persistent SST anomalies over the NW Pacific during JJA(1). In some models (NCEP and SINT) the decay of the cold SST anomaly on the southeastern flank of the anticyclone is very rapid and cooling is not seen in summer. All models including MME and observations illustrate that

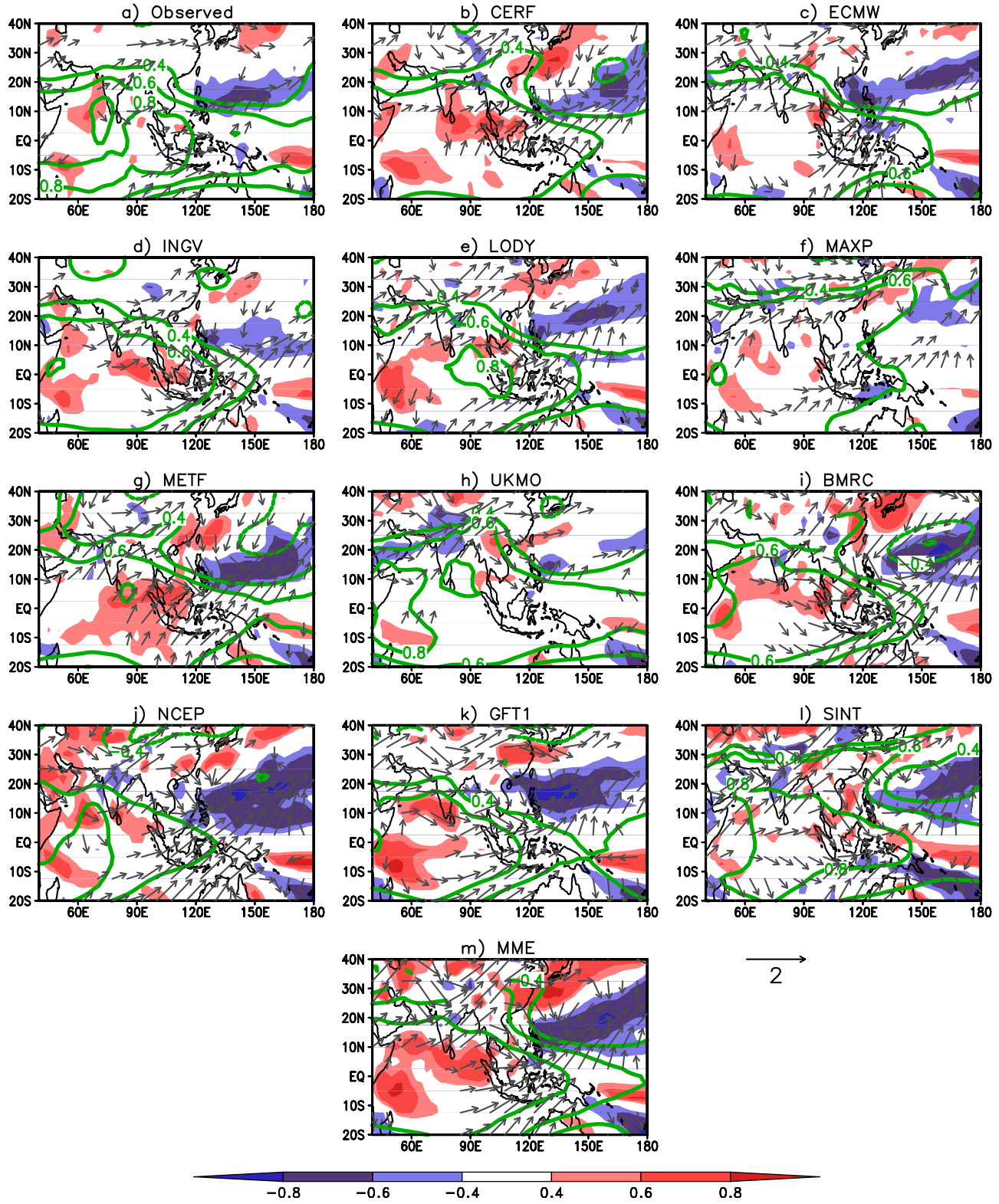

Figure 5. NDJ(0) Niño-3.4 SST index correlation with JJA(1) precipitation (shaded), tropospheric temperature (contours), and 200 hPa wind velocity (vectors) for (a) observations, (b–l) individual models, and (m) MME at 1 month lead prediction.

wind speed correlation is positive over the NW Pacific and negative over the NIO and north of the Maritime Continent (Figure 6). This indicates that easterly anomalies help cool NW Pacific SST and warms north of the Maritime Continent by altering the seasonal variation in the mean winds. In a few models in which local cool SST anomalies are weak (NCEP

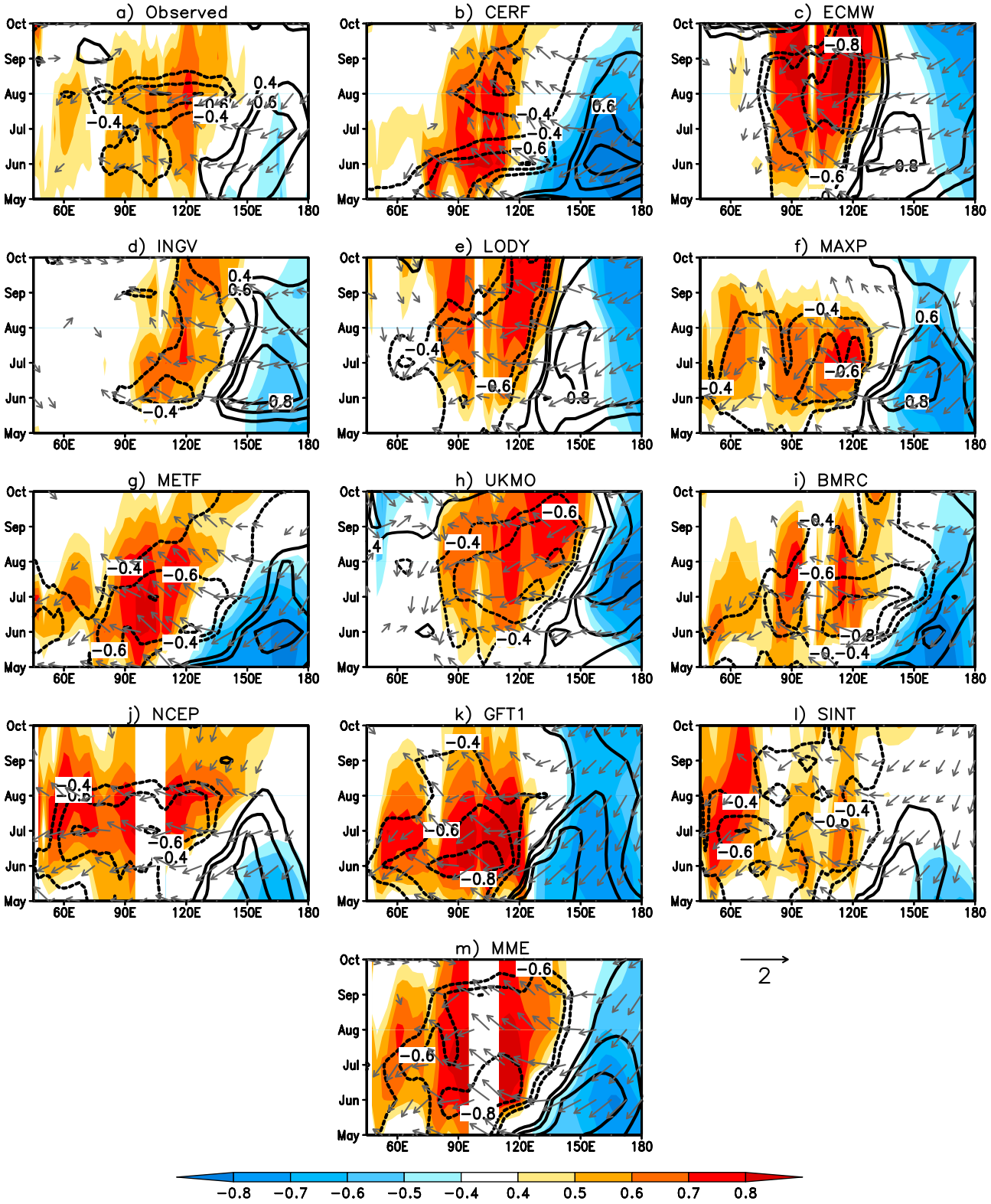

Figure 6. Correlation of SST (shaded), 850 hPa wind speed (contours), and wind anomalies (vectors) averaged from 5°N to 20°N with the NW Pacific SLP PC-1 for (a) observations, (b–l) individual models, and (m) MME initialized on 1 May. The *y* axis is the calendar month during the decay phase of El Niño.

and SINT), winds speed correlation is significant only in early summer over the NW Pacific region. In some models (CERF, METF, BMRC, GFT1 and MME) positive correlations are strong and sustained for entire summer season. Warming in north of the Maritime Continent and NIO are concur with low wind speed correlations in most models. During JJA(1),

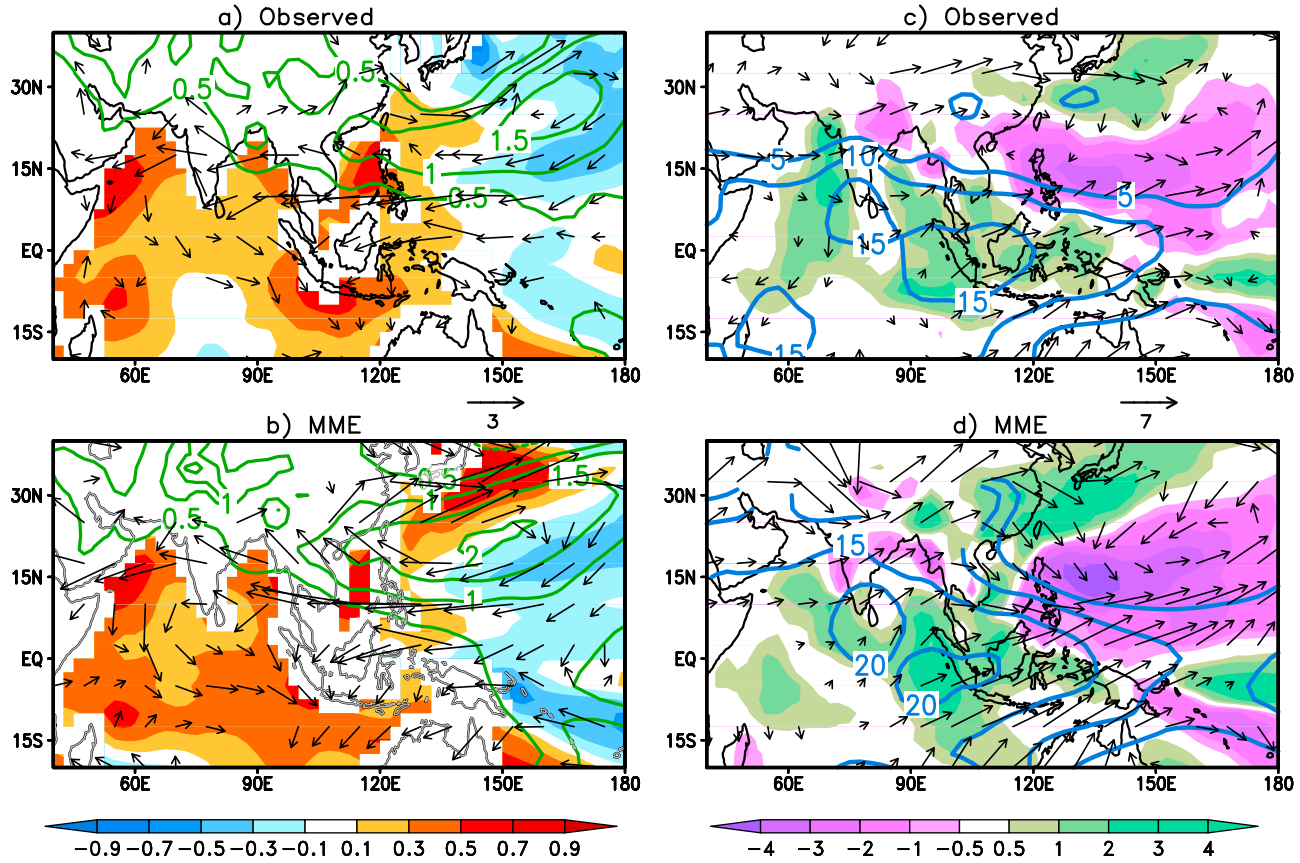

Figure 7. Composites of SST (shaded; °C), SLP (contours; hPa) and 850 hPa wind anomalies (vectors; above 0.3 m s^{-1} are displayed) during summer following El Niño (a) in observations and (b) in the MME. (c and d) Same as in Figures 7a and 7b but for precipitation (shaded; above 0.5 mm/d and below −0.5 mm/d are displayed), tropospheric temperature (TT) anomalies (contours, gpm), and 200 hPa wind anomalies (vectors; above 1 m s^{-1} are displayed). The summer seasons of 1983, 1992, and 1998 are selected for the composite analysis. MME is based on 1 month lead prediction.

changes in mean wind speed due to easterly wind anomalies over the NW Pacific and north of Maritime Continent might be the main reason for variations in SST among models.

[17] Figure 7 shows composites of JJA(1) anomalies for observations and for the MME predictions at a 1 month lead time constructed based on the NDJ(0) Niño-3.4 index and TIO warming. Three summers with a significant TIO warming (1983, 1992 and 1998) are considered for the analysis. The choice of our ENSO index selects El Niño events of large amplitude over the eastern Pacific (EP). The basin-wide warming of the TIO is strong in response to EP El Niño, and persists until the next summer. The MME well reproduces the observed anomalies of circulation and rainfall with TIO and South China Sea warming and cooling over southeastern flank of the surface anticyclone similar to correlation analysis (Figures 4 and 5). Rainfall anomalies in the east equatorial Indian Ocean in Figure 5 is weak but positive, and they are quite strong in El Niño composites (Figure 7c). As correlation analysis considers both El Niño and La Niña events, rainfall signals are reduced in Figure 5 over the east equatorial Indian Ocean in observations.

4.2. Effect of the TIO Warming

[18] TIO warming during JJA(1) is a robust feature in both observations and all models. Multiple physical processes seem to contribute to NW Pacific JJA(1) precipitation variability from the TIO. The Kelvin WIED mechanism appears to be important in linking the TIO warming and NW Pacific atmospheric anomalies in summer following El Niño. A wedge-like warm Kelvin wave in TT propagates into the equatorial western Pacific in both observations (Figure 7c) and in the MME (Figure 7d) composites. This warm Kelvin wave, which is accompanied by low surface pressure centered on the equator, drives northeasterly winds on the northern flank of the Kelvin wave due to friction [*Xie et al.*, 2009]. The resulting surface divergence suppresses atmospheric convection in the subtropical NW Pacific, including anomalous anticyclonic circulation (Figures 7a and 7b). Note that surface winds are not available for some models and therefore, 850 hPa winds are used to represent the low-level anticyclonic circulation. Surface wind anomalies [see *Xie et al.*, 2009, Figure 6] display clear cross-baric flow down the pressure gradient on the northern flank of the Kelvin wave. This cross-baric flow is weak in Figures 7a and 7b, in which 850 hPa winds are used. In most models and in the MME,

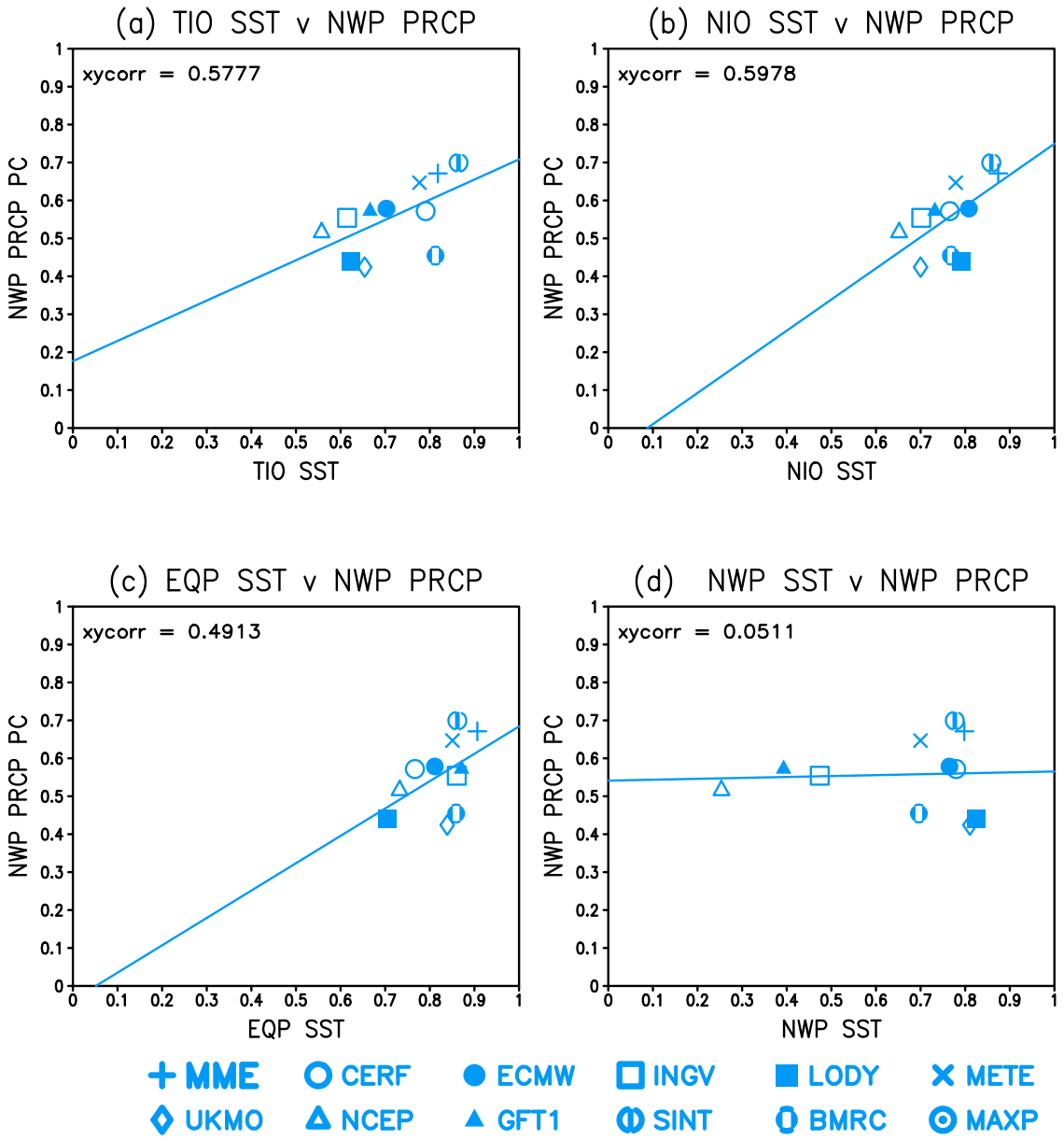

Figure 8. Scatter diagram between the forecast skill of JJA NW Pacific precipitation PC-2 and skill of regional SST area averaged time series over (a) the TIO (20°S–20°N and 45°E–100°E), (b) the NIO SST (0°–20°N and 50°E–97°E), (c) the equatorial Pacific (10°S–10°N and 120°E–90°W), and (d) the NW Pacific (0°–30°N and 130°E–180°E). All based on 1 month lead predictions. Note that skill score is based on correlation between observations and model time series.

the 1 month lead prediction displays an atmospheric Kelvin wave structure in SLP and TT (Figures 4, 5 and 7).

[19] In addition to the mechanism suggested by *Xie et al.* [2009], the TIO SST warming also affects the upper air circulation over the Northern Hemisphere westerly jet (Figures 7c and 7d and Figure 5). The subtropical westerly jet intensifies on the northern flank of the TT warming induced by the positive SST anomalies over the TIO. The intensified westerly jet in the upper troposphere (500~200 hPa) could enhance atmospheric convection over the Meiyu/Baiu rainband by advecting warm temperature from the Tibetan plateau region [*Sampe and Xie*, 2010]. The warm advection in the midtroposphere is balanced by adiabatic cooling in upward motion. The adiabatic-induced ascent favors convection in the presence of convective instability [*Sampe and Xie*, 2010]. The subtropical jet may also interact with the Pacific-Japan (PJ) pattern [*Nitta*, 1987; *Kosaka and Nakamura*, 2006] via convective-circulation interaction. A surface circulation in response to enhanced Meiyu-Baiu convection would induce surface wind divergence in the subtropics and suppress convection there. The response of the upper tropospheric circulation is found to be consistent with observations (Figure 5), especially in the MME composite analysis (Figure 7d). Thus, both the Kelvin WIED and westerly jet intensification mechanisms would help to sustain strong low-level anticyclonic anomalies in the subtropical NW Pacific, accompanied by

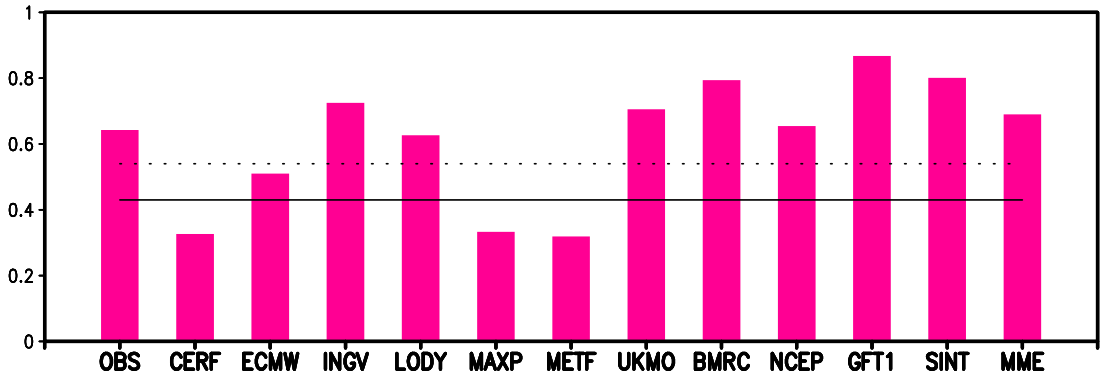

Figure 9. Correlation between JJ (June and July) NIO SST PC-1 and NW Pacific precipitation PC-2 for observations, individual models, and MME. All models based on 4 month lead prediction initialized on 1 February. Solid and dotted lines represent 95% and 99% confident levels, respectively.

enhanced rainfall over East Asia to the north. The Indian Ocean dipole mode may have a delayed effect on the summer monsoon over the NW Pacific and East Asia via the memory effect of eastern Eurasian snow [*Kripalani et al.*, 2010].

[20] To explore the remote SST forcing, Figure 8 shows the scatter diagram of NW Pacific rainfall PC-2 skill and area averaged SST anomaly skill of several regions. Skill score is based on the correlation between observations and models time series, indicating that models ability in predicting different regional SST anomalies. With low skill in the prediction of NW Pacific rainfall, MAXP model is not used here. Over all, there is a strong correlation in skill between SST anomalies over TIO/NIO and NW Pacific rainfall predictability. Models that are skillful in capturing TIO/NIO SST anomalies are likely to be successful in predicting NW Pacific rainfall variability. The simultaneous correlation between NW Pacific rainfall and equatorial Pacific PC skill scores is relatively low (Figure 8c). While the correlation between local SST and rainfall skill is almost zero among models (Figure 8d). The substantial differences in NW Pacific rainfall correlation with TIO, equatorial Pacific and local SST reaffirm the teleconnection effect of TIO SST variability on Pacific climate. [*Annamalai et al.*, 2005; *Kug et al.*, 2006; *Yang et al.*, 2007, 2009; *Xie et al.*, 2009; *Schott et al.*, 2009; *Huang et al.*, 2010].

5. Impact of Spring Asymmetric Mode on Long-Lead Prediction

[21] The NIO SST warming helps to force the warm tropospheric Kelvin wave that affects the circulation and convection over the NW Pacific during JJA(1) [*Xie et al.*, 2009]. Figure 9 shows that the correlation coefficient between the leading NIO (0°–20°N and 50°E–100°E) SST PC and the second NW Pacific (5°N–30°N and 100°E–180°E) rainfall PC corresponding to summer following El Niño is 0.64 for observations and 0.68 for the MME 4 month lead prediction (Here summer refers to June and July: In the 4 month lead prediction, average of June and July is used as summer season. This is because out of 11 models, 8 models (7 DEMETER and SINTEX-F) have retrospective forecasts (hindcasts) with 6 month integrations. For long-lead predictions hindcasts initialized in 1 February end on 31 July.) Thus, it is important to examine how the TIO/NIO SST warming evolves in long-lead predictions. Some models underestimate the relationship between NIO SST and NW Pacific precipitation compared to observations (e.g., MAXP and METF).

[22] The TIO displays coherent SST warming both north and south of the equator during summer following El Niño [*Yang et al.*, 2007; *Xie et al.*, 2009; *Du et al.*, 2009]. Ocean dynamics along with anomalous heat fluxes are responsible for the southwest tropical Indian Ocean (SWIO) warming at the peak phase of El Niño, and this warming persists until the following summer due to the slow propagation of downwelling Rossby waves [*Xie et al.*, 2002]. Figure 10 shows the regression of TIO SST and winds averaged zonally between 40°E and 100°E for observations and models initialized on 1 February, upon the NDJ(0) Niño-3.4 SST index in hindcasts. The SWIO displays maximum sea surface warming in spring and persists into JJA(1). Over the NIO, the SST increase exhibits peculiar double peak pattern, one centered in late boreal fall just prior to the peak of El Niño (not shown) and one in JJA(1) when El Niño has dissipated (Figure 10a). The strong SWIO warming induces an antisymmetric wind pattern in spring and early summer with anomalous northeasterlies north and southwesterlies south of the equator, respectively [*Wu et al.*, 2008; *Du et al.*, 2009]. In the early summer, the anomalous northeasterly anomalies oppose the mean southwesterlies and give rise to the pronounced second NIO peak in warming (Figure 10). This indicates that seasonal variations in mean wind are important for the interaction of easterly wind anomalies and SST. A few models have problems in predicting the second warming peak in June and July (LODY, MAXP, METF) correctly. Overall, most models are able to predict the June and July (JJ) second warming peak over the NIO, suggesting that air-sea interactions over this region at long lead are well represented (Figure 9). Similar to 1 month lead prediction (Figure 8b), at 4 month lead, the scatter diagram between JJ(1) skills of NW Pacific rainfall PC-2 and NIO SST shows positive correlation among models (not shown). This illustrates the importance of NIO SST for predicting the NW Pacific summer rainfall at long-lead prediction.

[23] Figure 11 shows March–May (MAM) rainfall EOF-1 over the TIO for observations and for 1 month lead model predictions initialized on 1 February. During boreal spring over the TIO, an asymmetric pattern in rainfall develops

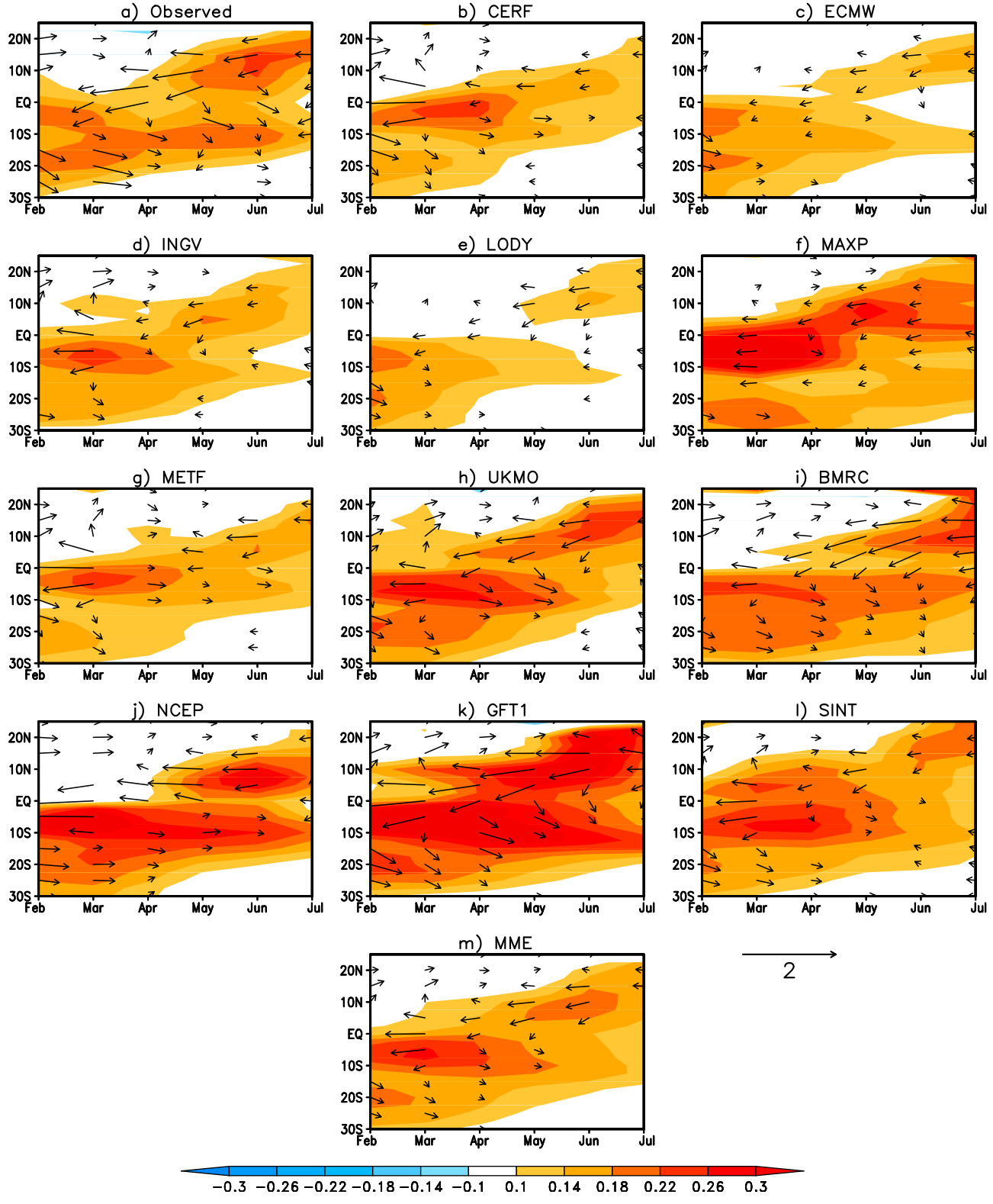

Figure 10. Regression of SST (shaded; °C) and 850 hPa wind anomalies (vectors; m s^{-1}) averaged zonally between 40°E and 100°E, against the observed NDJ(0) Niño-3.4 SST index for (a) observations, (b–l) individual models, and (m) the MME initialized on 1 February. The *x* axis is the calendar month during the decay phase of El Niño.

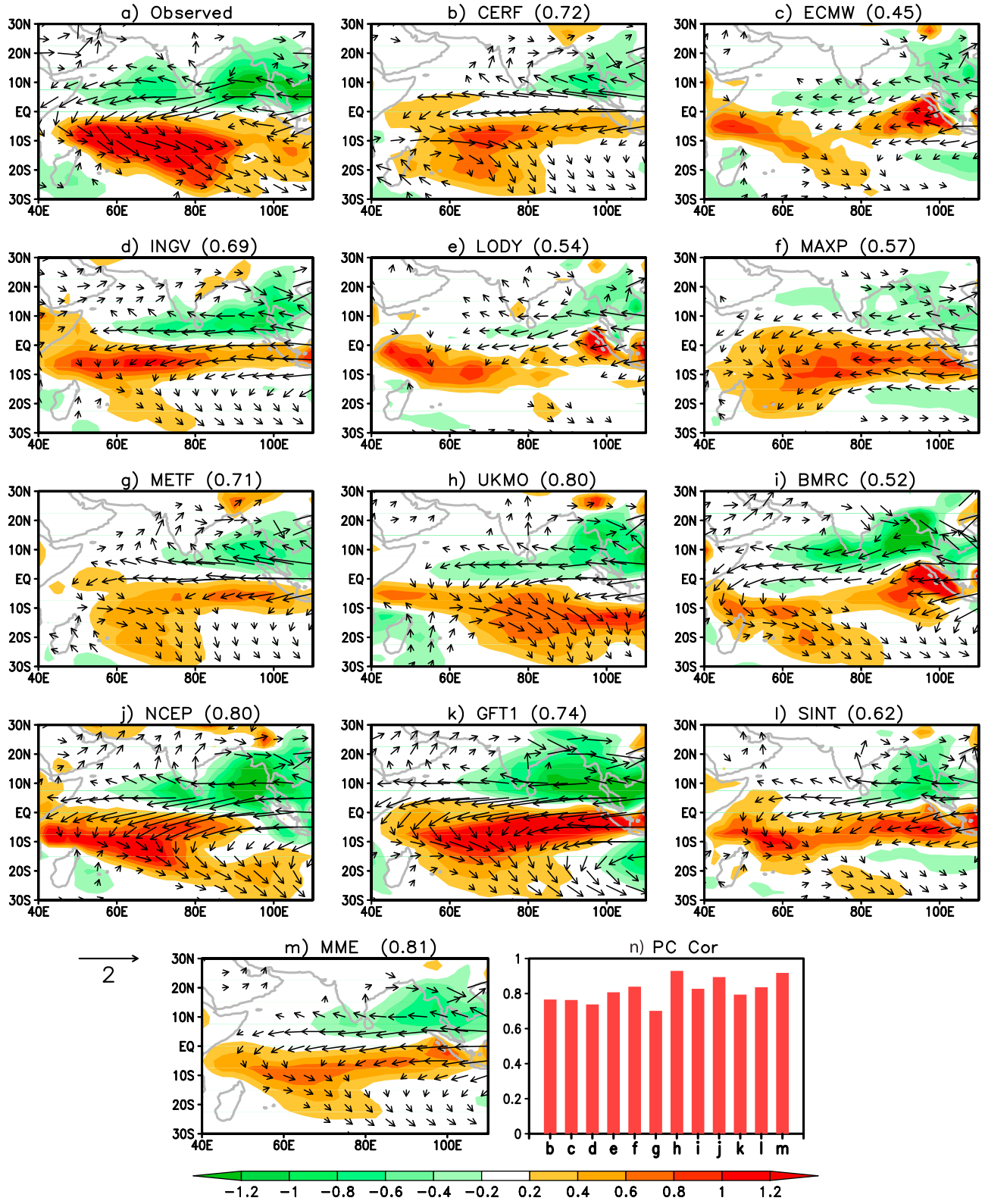

Figure 11. The first EOF of MAM precipitation (shaded; mm/d) variability for (a) observations, (b–l) models, and (m) MME for 1 month lead predictions. (m) Temporal correlation for precipitation PCs between models and observations over the TIO. In Figures 11a–11m, vectors represent the 850 hPa wind anomalies (m s^{-1}) regressed upon corresponding rainfall PC. The pattern correlation between the observed and predicted EOFs is shown at the top of Figures 11b–11m.

with negative anomalies north of the equator and positive anomalies to the south [*Wu et al.*, 2008; *Xie et al.*, 2009; *Du et al.*, 2009; *Wu and Yeh*, 2010]. The predictability of the asymmetric mode in rainfall is high, as shown in both spatial and temporal correlations. In particular, the temporal correlation exceeds 0.75 for individual models and reaches 0.9 for the MME (Figure 11n). Winds regressed upon the MAM rainfall PC show robust northeasterly anomalies that are subsequently important for developing the second warming over the NIO in the early summer via surface heat flux adjustments [*Du et al.*, 2009]. Like rainfall and winds, the pattern of MAM SST anomalies is similar between observations and models (figure not shown).

[24] The asymmetric mode of wind and precipitation is weak in those models (Figure 11), that tend to predict weak SST warming over the NIO in early summer (Figure 10) (e.g., CERF, ECMW and LODY). We note that the models that predict weak northeasterlies north of the equator have relatively low skill in predicting the relationship between NIO JJ(1) SST and NW Pacific rainfall (e.g., CERF, ECMW, MAXP and METF: Figures 11 and 9). Overall prediction skill scores are high for the MAM(1) antisymmetric rainfall/wind pattern and summer NIO peak.

6. Summary

[25] We have evaluated the NW Pacific summer climate predictability in 11 climate models for a 22 year period of 1980–2001. Analysis of coupled models and the associated MME at prediction lead times of 1 month reveal that the first EOF mode of SLP is closely linked to the second EOF mode of rainfall variability over the NW Pacific during the summer following El Niño. The correlation of corresponding PCs over the NW Pacific is 0.8 for observations and 0.95 for the MME prediction. Most coupled models and MME well predict these EOF modes and their interrelationships. Coupled models that produce a high correlation between the SLP and rainfall PCs tend to have high skill in predicting the second EOF mode of rainfall, illustrating the importance of circulation-convection feedback. The temporal correlation between the predicted and observed rainfall PCs stays above the 95% significance level in most models. The MME showed superior skill (r = 0.7) in terms of rainfall EOF pattern correlation compared with individual models during JJA(1). The PC skill score of SLP over the NW Pacific are better than those of precipitation in many models.

[26] A few models (four out of eleven) do not feature weak negative SST anomalies over the NW Pacific but are able to forecast the suppressed rainfall, suggesting that the remote forcing is important for precipitation prediction over the NW Pacific region in these models. Some models (CERF, METF, BMRC, GFT1) display relatively strong cooling on the southeastern flank of the anomalous anticyclone compared to observations. The SST cooling suppresses convection and reduces latent heat release and excites a descending atmospheric Rossby wave and reinforces the NW Pacific anticyclone [*Wang et al.*, 2000, 2003]. However, local SST cooling decays very rapidly as the monsoon progresses, whereas TIO warming decays gradually after summer.

[27] Our analysis of multimodel hindcasts supports the notion that the TIO SST anomaly affects NW Pacific climate, whereas the equatorial Pacific and local SST effect on the NW Pacific is weak in JJA(1). Two mechanisms are identified for TIO to affect NW Pacific rainfall variability during JJA(1). One is the Kelvin wave-induced Ekman divergence mechanism [*Xie et al.*, 2009] and the other is the intensification of the subtropical westerly jet, both in response to the TIO warming. The latter is a new hypothesis derived from the present study. Tropospheric temperature increases with a broad meridional structure, leading to the intensification of the subtropical westerly jet on the northern flank. The intensified westerly jet could enhance the convection over the Meiyu/Baiu rainband by warm temperature advection [*Sampe and Xie*, 2010]. The resultant low SLP drives surface wind divergence to the south over the subtropical NW Pacific, suppressing convection in the latter region. To predict NW Pacific atmospheric anomalies during JJA(1), our result show that models need to predict the TIO SST and precipitation well along with SST cooling on the southeastern flank of the anticyclone. A better understanding of interannual/JJA(1) NW Pacific variability and the impact of the TIO warming on atmospheric circulation, however, seems essential to improve seasonal forecasts.

[28] In most models, the leading mode in spring rainfall over TIO is antisymmetric about the equator and well represented in 1 month lead predictions initialized from 1 February over the TIO. To our knowledge, this study is first to show model skill in predicting spring anomalies over the TIO. Many models display a second peak in SST warming over the NIO during early summer after El Niño (June–July) when initialized from 1 February (4 month lead prediction). Models that predict the second peak in NIO SST anomalies have good skill in predicting NW Pacific negative rainfall anomalies in the subsequent summer (BMRC and GFDL). The MME analysis generally supports previous findings regarding the TIO capacitor effect based on a single model [*Chowdary et al.*, 2010] and observational studies [*Xie et al.*, 2009; *Du et al.*, 2009]. Because the NW Pacific rainfall in summer is not correlated with local SST, the predictability of the atmospheric anomalies over this region owes largely to SST anomalies elsewhere, especially those over the TIO. How to quantify the impact of SST anomalies over TIO, local and other tropical oceans on summer NW Pacific climate still needs further investigation.

[29] **Acknowledgments.** This work is supported by the U.S. National Science Foundation, the Japan Agency for Marine-Earth Science and Technology, and the National Aeronautics and Space Administration (NASA). We thank anonymous reviewers for their valuable comments that helped to improve our manuscript and H. Annamalai for helpful discussions. We acknowledge Nat Johnson, Jan Hafner, and P. A. Prasanth for their help and corrections. Lee and Wang acknowledge support from APEC Climate Center (APCC) and the Korean Meteorological Administration Research and Development Program under grant RACS 2010–2017. Figures are prepared in Grads. IPRC/SOEST publication 716/8005.

References

Annamalai, H., P. Liu, and S.-P. Xie (2005), Southwest Indian Ocean SST variability: Its local effect and remote influence on Asian monsoons, *J. Clim.*, *18*, 4150–4167, doi:10.1175/JCLI3533.1.

Chang, C. P., Y. Zhang, and T. Li (2000), Interannual and interdecadal variations of the East Asian summer monsoon and tropical Pacific SSTs. Part I: Roles of the subtropical ridge, *J. Clim.*, *13*, 4310–4325, doi:10.1175/1520-0442(2000)013<4310:IAIVOT>2.0.CO;2.

Chowdary, J. S., S.-P. Xie, J.-J. Luo, J. Hafner, S. Behera, Y. Masumoto, and T. Yamagata (2010), Predictability of Northwest Pacific climate dur-

ing summer and the role of the tropical Indian Ocean, *Clim. Dyn.*, doi:10.1007/s00382-009-0686-5, in press.

Delworth, T. L., et al. (2006), GFDL's CM2 global coupled climate models—Part I: Formulation and simulation characteristics, *J. Clim.*, *19*, 643–674, doi:10.1175/JCLI3629.1.

Du, Y., S.-P. Xie, G. Huang, and K. Hu (2009), Role of air-sea interaction in the long persistence of El Niño-induced North Indian Ocean warming, *J. Clim.*, *22*, 2023–2038, doi:10.1175/2008JCLI2590.1.

Gill, A. E. (1980), Some simple solutions for heat-induced tropical circulation, *Q. J. R. Meteorol. Soc.*, *106*, 447–462, doi:10.1002/qj.49710644905.

Huang, G., K. Hu, and S.-P. Xie (2010), Strengthening of tropical Indian Ocean teleconnection to the northwest Pacific since the mid-1970s: An atmospheric GCM study, *J. Clim.*, *19*, 5294–5304, doi:10.1175/2010JCLI3577.1, in press.

Huang, R., W. Chen, B. Yang, and R. Zhang (2004), Recent advances in studies of the interaction between the East Asian winter and summer monsoons and ENSO cycle, *Adv. Atmos. Sci.*, *21*, 407–424, doi:10.1007/BF02915568.

Hudson, D., O. Alves, H. H. Hendon, and G. Wang (2010), The impact of atmospheric initialisation on seasonal prediction of tropical Pacific SST, *Clim. Dyn.*, doi:10.1007/s00382-010-0763-9, in press.

Kanamitsu, M., W. Ebisuzaki, J. Woollen, S.-K. Yang, J. J. Hnilo, M. Fiorino, and G. L. Potterl (2002), NCEP-DOE AMIP-II Reanalysis (R-2), *Bull. Am. Meteorol. Soc.*, *83*, 1631–1643, doi:10.1175/BAMS-83-11-1631(2002)083<1631:NAR>2.3.CO;2.

Klein, S. A., B. J. Soden, and N.-C. Lau (1999), Remote sea surface temperature variations during ENSO: Evidence for a tropical atmospheric bridge, *J. Clim.*, *12*, 917–932, doi:10.1175/1520-0442(1999)012<0917:RSSTVD>2.0.CO;2.

Kosaka, Y., and H. Nakamura (2006), Structure and dynamics of the summertime Pacific-Japan (PJ) teleconnection pattern, *Q. J. R. Meteorol. Soc.*, *132*, 2009–2030, doi:10.1256/qj.05.204.

Kripalani, R. H., J. H. Oh, and H. S. Chaudhari (2010), Delayed influence of the Indian Ocean Dipole mode on the East Asia–West Pacific monsoon: Possible mechanism, *Int. J. Climatol.*, *30*, 197–209, doi:10.1002/joc.1890.

Kug, J.-S., T. Li, S.-I. An, I.-S. Kang, J.-J. Luo, S. Masson, and T. Yamagata (2006), Role of the ENSO-Indian Ocean coupling on ENSO variability in a coupled GCM, *Geophys. Res. Lett.*, *33*, L09710, doi:10.1029/2005GL024916.

Lau, N.-C., and M. J. Nath (2003), Atmosphere-ocean variations in the Indo-Pacific sector during ENSO episodes, *J. Clim.*, *16*, 3–20, doi:10.1175/1520-0442(2003)016<0003:AOVITI>2.0.CO;2.

Lee, E., T. N. Chase, and B. Rajagopalan (2008), Seasonal forecasting of East Asian summer monsoon based on oceanic heat sources, *Int. J. Climatol.*, *28*, 667–678, doi:10.1002/joc.1551.

Lee, J.-Y., et al. (2010), How are seasonal prediction skills related to models' performance on mean state and annual cycle?, *Clim. Dyn.*, *35*, 267–283, doi:10.1007/s00382-010-0857-4(3).

Li, S., J. Lu, G. Huang, and K. Hu (2008), Tropical Indian Ocean basin warming and East Asian summer monsoon: A multiple AGCM study, *J. Clim.*, *21*, 6080–6088, doi:10.1175/2008JCLI2433.1.

Lu, R. (2001), Interannual variability of the summertime North Pacific subtropical high and its relation to atmospheric convection over the warm pool, *J. Meteorol. Soc. Jpn.*, *79*, 771–783, doi:10.2151/jmsj.79.771.

Luo, J.-J., S. Masson, S. Behera, S. Shingu, and T. Yamagata (2005), Seasonal climate predictability in a coupled OAGCM using a different approach for ensemble forecast, *J. Clim.*, *18*, 4474–4497, doi:10.1175/JCLI3526.1.

Matsuno, T. (1966), Quasi-geostrophic motions in the equatorial area, *J. Meteorol. Soc. Jpn.*, *44*, 25–43.

Nitta, T. (1987), Convective activities in the tropical western Pacific and their impact on the Northern Hemisphere summer circulation, *J. Meteorol. Soc. Jpn.*, *65*, 373–390.

Palmer, T. N., et al. (2004), Development of a European multi-model ensemble system for seasonal to interannual prediction (DEMETER), *Bull. Am. Meteorol. Soc.*, *85*, 853–872, doi:10.1175/BAMS-85-6-853.

Park, H. S., J. C. Chiang, B. R. Lintner, and G. J. Zhang (2010), The delayed effect of major El Niño events on Indian monsoon rainfall, *J. Clim.*, *23*, 932–946, doi:10.1175/2009JCLI2916.1.

Rayner, N. A., D. E. Parker, E. B. Horton, C. K. Folland, L. V. Alexander, D. P. Rowell, E. C. Kent, and A. Kaplan (2003), Global analyses of sea surface temperature, sea ice, and night marine air temperature since the late nineteenth century, *J. Geophys. Res.*, *108*(D14), 4407, doi:10.1029/2002JD002670.

Saha, S., et al. (2006), The NCEP Climate Forecast System, *J. Clim.*, *19*, 3483–3517, doi:10.1175/JCLI3812.1.

Sampe, T., and S.-P. Xie (2010), Large-scale dynamics of the Meiyu-Baiu rain band: Environmental forcing by the westerly jet, *J. Clim.*, *23*, 113–134, doi:10.1175/2009JCLI3128.1.

Schott, F. A., S.-P. Xie, and J. P. McCreary (2009), Indian Ocean circulation and climate variability, *Rev. Geophys.*, *47*, RG1002, doi:10.1029/2007RG000245.

Shen, X., M. Kimoto, A. Sumi, A. Numaguti, and J. Matsumoto (2001), Simulation of the 1998 East Asian summer monsoon by the CCSR/NIES AGCM, *J. Meteorol. Soc. Jpn.*, *79*, 741–757, doi:10.2151/jmsj.79.741.

Wang, B., and Q. Zhang (2002), Pacific-East Asian teleconnection, part II: How the Philippine Sea anticyclone established during development of El Nino, *J. Clim.*, *15*, 3252–3265, doi:10.1175/1520-0442(2002)015<3252:PEATPI>2.0.CO;2.

Wang, B., R. Wu, and X. Fu (2000), Pacific-east Asian teleconnection: How does ENSO affect east Asian climate?, *J. Clim.*, *13*, 1517–1536, doi:10.1175/1520-0442(2000)013<1517:PEATHD>2.0.CO;2.

Wang, B., R. Wu, and T. Li (2003), Atmosphere-warm ocean interaction and its impacts on the Asian-Australian monsoon variation, *J. Clim.*, *16*, 1195–1211, doi:10.1175/1520-0442(2003)16<1195:AOIAII>2.0.CO;2.

Wang, B., I.-S. Kang, and J.-Y. Lee (2004), Ensemble simulations of Asian-Australian monsoon variability by 11 AGCMs, *J. Clim.*, *17*, 803–818, doi:10.1175/1520-0442(2004)017<0803:ESOAMV>2.0.CO;2.

Wang, B., Q. Ding, X. Fu, I.-S. Kang, K. Jin, J. Shukla, and F. Doblas-Reyes (2005), Fundamental challenge in simulation and prediction of summer monsoon rainfall, *Geophys. Res. Lett.*, *32*, L15711, doi:10.1029/2005GL022734.

Wang, B., J. Yang, T. Zhou, and B. Wang (2008), Interdecadal changes in the major modes of Asian-Australian monsoon variability: Strengthening relationship with ENSO since the late 1970s, *J. Clim.*, *21*, 1771–1789, doi:10.1175/2007JCL1981.1.

Wang, B., et al. (2009), Advance and prospect of seasonal prediction: Assessment of the APCC/CliPAS 14-model ensemble retrospective seasonal prediction (1980–2004), *Clim. Dyn.*, *33*, 93–117, doi:10.1007/s00382-008-0460-0.

Wu, B., T. Li, and T. Zhou (2010), Relative contributions of the Indian Ocean and local SST anomalies to the maintenance of the western North Pacific anomalous anticyclone during El Niño decaying summer, *J. Clim.*, *23*, 2974–2986, doi:10.1175/2010JCLI3300.1.

Wu, R., and S. W. Yeh (2010), A further study of the tropical Indian Ocean asymmetric mode in boreal spring, *J. Geophys. Res.*, *115*, D08101, doi:10.1029/2009JD012999.

Wu, R., B. P. Kirtman, and V. Krishnamurthy (2008), An asymmetric mode of tropical Indian Ocean rainfall variability in boreal spring, *J. Geophys. Res.*, *113*, D05104, doi:10.1029/2007JD009316.

Xie, P., and P. A. Arkin (1996), Analyses of global monthly precipitation using gauge observations, satellite estimates, and numerical model predictions, *J. Clim.*, *9*, 840–858, doi:10.1175/1520-0442(1996)009<0840:AOGMPU>2.0.CO;2.

Xie, S.-P., H. Annamalai, F. A. Schott, and J. P. McCreary (2002), Structure and mechanisms of South Indian Ocean climate variability, *J. Clim.*, *15*, 864–878, doi:10.1175/1520-0442(2002)015<0864:SAMOSI>2.0.CO;2.

Xie, S.-P., K. Hu, J. Hafner, Y. Du, G. Huang, and H. Tokinaga (2009), Indian Ocean capacitor effect on Indo-western Pacific climate during the summer following El Niño, *J. Clim.*, *22*, 730–747, doi:10.1175/2008JCLI2544.1.

Xie, S.-P., Y. Du, G. Huang, X.-T. Zheng, H. Tokinaga, K. Hu, and Q. Liu (2010), Interdecadal change of the 1970s in El Niño influences on Indo-western Pacific and East Asian climate, *J. Clim.*, *23*, 3352–3368, doi:10.1175/2010JCLI3429.1.

Yang, J., Q. Liu, S.-P. Xie, Z. Liu, and L. Wu (2007), Impact of the Indian Ocean SST basin mode on the Asian summer monsoon, *Geophys. Res. Lett.*, *34*, L02708, doi:10.1029/2006GL028571.

Yang, J., Q. Liu, Z. Liu, L. Wu, and F. Huang (2009), Basin mode of Indian Ocean sea surface temperature and Northern Hemisphere circumglobal teleconnection, *Geophys. Res. Lett.*, *36*, L19705, doi:10.1029/2009GL039559.

J. S. Chowdary, Y. Kosaka, J.-Y. Lee, B. Wang, and S.-P. Xie, International Pacific Research Center, University of Hawaii at Manoa, 1680 East-West Rd., Honolulu, HI 96822, USA. (sriranga@hawaii.edu)